Advanced Steel Construction – Vol. 20 No. 3 (2024) 300–309
DOI:10.18057/IJASC.2024.20.3.9

BUCKLING MODES OF SCREWED CONNECTIONS IN COLD-FORMED STEEL BUILT-UP PLATES

Yan-Chun Li [1], Tian-Hua Zhou [2], Ai-Hong Han [1], Yan Lu [3, *] and Ji-Hao Chen [1]

[1] *School of Civil Engineering and Communication, North China University of Water Resources and Electric Power, Zhengzhou 450045, China*
[2] *School of Civil Engineering, Chang'an University, Xi'an 710061, China*
[3] *School of Civil Engineering, Inner Mongolia University of Technology, Hohhot 010051, China*
** (Corresponding author: E-mail: luyanchd@163.com)*

ABSTRACT

Discrete screws can introduce discontinuities at the interface of built-up plates, leading to various buckling modes in cold-formed steel (CFS) built-up plates, namely coordinated buckling and delamination buckling. The impact of these buckling deformation modes on the stability mechanism of CFS screw-connected built-up plates is significant and cannot be overlooked. Consequently, this paper establishes theoretical models for both buckling modes. Analytical solutions for the critical buckling stress (CBS) of the screw-connected built-up plate under these two modes are derived. The validity of the buckling modes and the analytical solutions is confirmed through experimental verification. The results indicate that: (1) delamination buckling is invariably a higher-order mode in comparison to coordinated buckling, and as such, only coordinated buckling is required for calculating the CBS; (2) the CBS calculation method proposed in this paper aligns more closely with the actual mechanical behavior of screw connections in CFS built-up plates.

ARTICLE HISTORY

Received: 20 January 2024
Revised: 27 February 2024
Accepted: 10 March 2024

KEYWORDS

Cold-formed steel;
Screwed connection of built-up plates;
Shear slip;
Coordinated buckling;
Delamination buckling;
Critical buckling stress

1. Introduction

Cold-formed steel (CFS) members are widely used domestically and internationally due to their flexible forming, simple production process, and high post-buckling strength. The built-up members assembled using self-drilling screws are commonly used in engineering circles. The stability of a single plate has been studied by Timoshenko [1] and the relatively perfect elastic stability theories have been established [2,3]. The CFS built-up members are being used to meet the increasing demand for practical projects in recent years. Self-drilling screws have gradually become one of the primary methods for connecting composite plates due to their simple construction, excellent connection stiffness, and high bearing capacity [4-6].

Therefore, scholars have studied the mechanical characteristics of CFS composite plates [7-9]. The results indicate that the shear capacity of self-drilling screw groups exhibits a "group reduction effect". Recently, the influences of screws on the high-strength (G550) CFS members were experimentally and numerically investigated [10]. Different behaviors that occur simultaneously in the screw connection test were successfully simulated: steel plate tearing and pulling out, end plate failure, screw tilting, and fracture. The shear behavior of the CFS plate connected by self-drilling screws was studied using experimental, numerical, and analytical models. Three typical failure modes were identified [11]. A model was proposed and calibrated to predict the shear deformation of the screw built-up plate. A revised reduction factor for the bearing capacity is presented based on the Australian Standard. The shear behavior of self-drilling screw connections in CFS plates was studied through experiments and numerical analysis. Three typical failure modes were identified through research, and it was found that these three failure modes are closely linked to the ratio of screw diameter to plate thickness [12]. Liu [13] conducted an experimental and numerical investigation of screwed connections of CFS plates, studying the shear strength and failure modes of the specimens. A calculation method for determining the bearing capacity was proposed. Screw connections have been extensively used in CFS constructions due to their convenient installation and high load-bearing capacity. A sophisticated finite element model was developed to analyze the pull-out performance of screw connections. It is indicated that the failure types of the specimen include screw hole compression failure and screw shear failure [14].

CFS is often assembled using screw fasteners because they can be easily drilled through thin sheets of steel [15-21]. However, individual screws can cause discontinuities in the interface of the built-up plate. Therefore, the impact of screws on CFS built-up members cannot be ignored. Ting et al. [22-24] conducted experimental and numerical simulation studies on the influence of screw arrangements and screw diameters on the bearing capacity of various types of CFS built-up members. Owing to the shear action of the screw [25], the buckling mode and failure type of the built-up part of the member will change compared to the member without the influence of the screw. Therefore, screws are an important factor that affects the capacity of the CFS built-up members. Additionally, the failure mode of the screw will also impact the ultimate capacity of the built-up member [26,27]. Previous studies have focused on the mechanical behavior of CFS built-up members. However, the research on the buckling mechanism and critical buckling stress (CBS) of composite members in CFS built-up structures is still incomplete.

The most significant feature of the SBP is the discontinuity of the connection interface. However, due to this structural property, the application of the small deflection theory in the SBP raises the following two problems that need to be considered:

(1) There may be either coordinated buckling with the same deformation direction or delamination buckling with the opposite deformation direction between each single plate due to the discontinuity of the connection interface between the SBP. It remains to be studied whether the delamination buckling is considered when studying the CBS of the SBP.

(2) The discontinuity in the screwed connection may cause the shear deformation of the SBP during buckling. However, the shear deformation can also be constrained extent by discrete screw fasteners. While the effects of shear deformation of the built-up plate and screw constraint are not reflected in the current design method for the CBS.

Therefore, this paper investigates the instability mechanism of the SBP by using a four-sided simply supported plate as an example. The SBP in this paper is extracted from the built-up webs in the CFS back-to-back built-up column, as presented in Fig. 1(a). The constraint of the flanges on the webs is assumed to be a simply supported edge. The connection between the column ends and the end plates through spot welding is also considered a simply supported boundary condition. Therefore, a screw built-up plate with simply supported on four sides is established, as shown in Fig. 1(b).

The possible instability deformation modes are analyzed, and the calculation models of different deformation modes are established by comparing the various buckling modes between the built-up plate and the single plate. The analytical expression of the CBS for the built-up plate was derived considering the effects of different deformation modes on the structural behavior of the plate. The influence of various deformation modes on the SBP is then examined to identify the specific instability mode of the built-up plate. Finally, the discussion explores the influences of boundary conditions on the instability modes of the SBP.

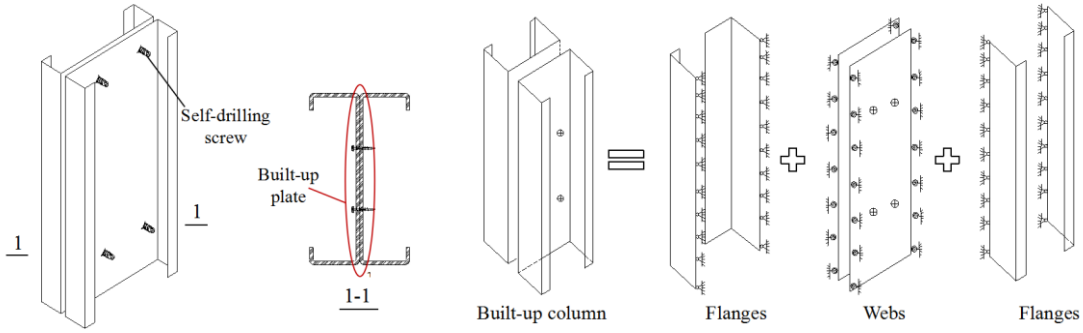

(a) Screw built-up plates (b) Boundary conditions

Fig. 1 The source of the SBP and the determination of the boundary conditions

2. Buckling deformation modes

To study the deformation modes of the simply supported on four sides SBP, this paper analyzes the following three cases: (1) SBP may experience coordinated buckling and delamination buckling, without considering the coordination action of the plate, as shown in Fig. 2(a). The opposite deformation occurs at the deformation area within the partial panels for the delamination buckling mode. (2) When considering the coordinated deformation between two single plates, the plates at the opposite deformation location of the delamination buckling will compress each other. This compression causes the bending deformations to cancel each other out, forming a straight section, as illustrated in Fig. 2 (b). (3) In practice, the plates at the screw area also have the same deflection direction and dimension out of plane due to the constraint of screws, as presented in Fig. 2(c). Therefore, it can be concluded that two main modes of instability deformation occur, namely coordinated buckling and delamination buckling for the SBP simply supported on four sides.

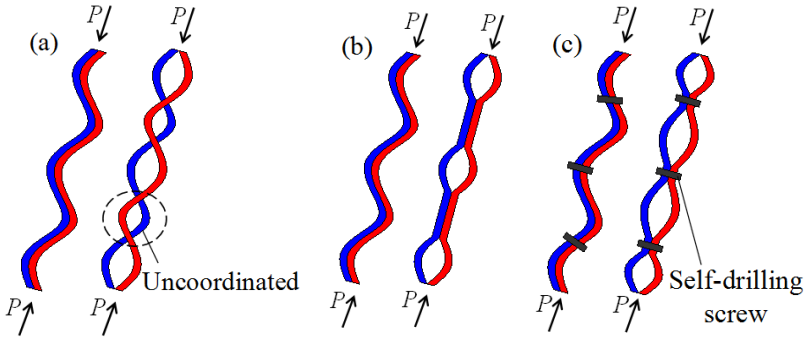

Fig. 2 Deformation modes of the SBP with four edges simply supported. ((a) Without considering the effect of plates; (b) Considering the effect of plates; (c) Considering the effect of plates and screws)

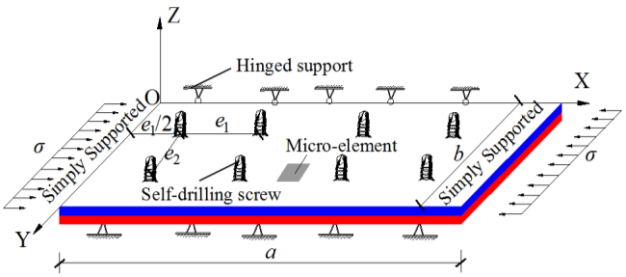

(a) The simplified model of the SBP

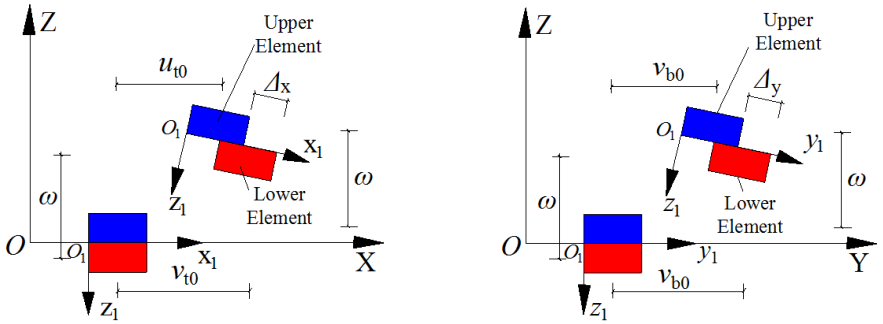

(b) Shear slip in the XOZ plane (c) Shear slip in the YOZ plane

Fig. 3 Calculation models of the SBP with four edges simply supported

3. Buckling modes

3.1. Coordinate buckling mode

3.1.1. Calculation model

A computational model of the CBS for the coordinated buckling deformation mode is presented in Fig. 3. The model consists of two identical plates connected by self-drilling screws, as shown in Fig. 3(a). A micro-element is extracted from the SBP to analyze the buckling deformation relationship between the upper and lower plates, as presented in Figs. 3(a)-3(c). Additionally, the overall coordinate system and local coordinate systems are established in Figs. 3(b)-3(c) to analyze the mechanical behavior between two individual plates in detail. Figs. 3(b) and 3(c) demonstrate the mechanical behaviors of the SBP during buckling in the XOZ plane and YOZ plane, respectively. At the connection interface for the built-up plate, coordinate systems $x_1o_1z_1$ and $y_1o_1z_1$ are established for follow-up purposes, as shown in Fig. 3(b)-3(c). The theoretical derivation can then be developed based on the energy method. Therefore, the following two basic assumptions are made for the convenience of the mathematical modeling.

(1) The influence of the size of the screw hole on the stability of the built-up plate is disregarded because the diameter of self-drilling screws being much smaller than the plate width.

(2) The constraint of self-drilling screws on the shear deformation of SBP can be simplified as shown in Fig. 4. The imaginary shear body is only subjected to shear deformation.

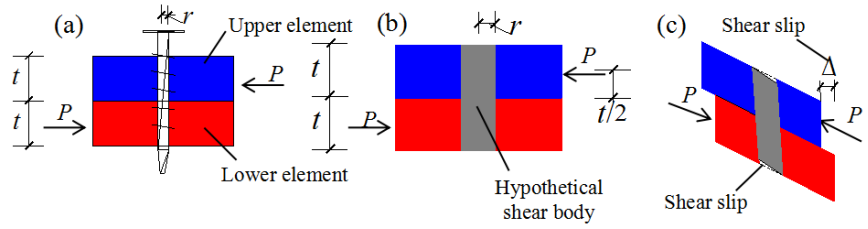

Note：P is the pressure acting on the middle surface of each veneer

Fig. 4 Mechanism behaviors of the ((a) Micro-element of the SBP; (b) Hypothetical shear body of screws; (c) Shear slip deformation)

3.1.2. The mechanism behaviors of the micro-element

According to Fig. 3 and the assumption (1), the displacement of any point on the upper element is:

$$u_t = u_{t0} - (z_1 + t/2)\frac{\partial \omega}{\partial x} \tag{1a}$$

$$v_t = v_{t0} - (z_1 + t/2)\frac{\partial \omega}{\partial y} \tag{1b}$$

where, u_t and v_t represent the displacement of the upper element along the X-axis and the Y-axis directions of the global coordinate system, respectively. ω represents the deflection along the Z-axis direction of the global coordinate system. z_1 represents the displacement in the z_1 direction of the follow-up coordinate system.

Similarly, the displacement of any point of the lower elements is:

$$u_b = u_{b0} - (z_1 - t/2)\frac{\partial \omega}{\partial x} \tag{1c}$$

$$v_b = v_{b0} - (z_1 - t/2)\frac{\partial \omega}{\partial y} \tag{1d}$$

where u_b and v_b represent the displacement of the lower element along the X-axis and the Y-axis directions of the global coordinate system, respectively.

The strain of each element is then derived from the formulas (1a) to (1d):

$$\varepsilon_{xt} = \frac{\partial u_{t0}}{\partial x} - (z_1 + t/2)\frac{\partial^2 \omega}{\partial x^2} \tag{2a}$$

$$\varepsilon_{yt} = \frac{\partial v_{t0}}{\partial y} - (z_1 + t/2)\frac{\partial^2 \omega}{\partial y^2} \tag{2b}$$

$$\varepsilon_{xb} = \frac{\partial u_{b0}}{\partial x} - (z_1 - t/2)\frac{\partial^2 \omega}{\partial x^2} \tag{2c}$$

$$\varepsilon_{vb} = \frac{\partial v_{b0}}{\partial y} - (z_1 - t/2)\frac{\partial^2 \omega}{\partial y^2} \tag{2d}$$

where, ε_{xt}、 ε_{xt} and ε_{xb}、 ε_{xb} are the strains of any point of the upper element and lower element along the X-axis and the Y-axis directions of the global coordinate system, respectively.

Therefore, the normal stress of the upper and lower elements is obtained according to Hooke's law [1]:

$$\sigma_{xt} = \frac{E}{1-\nu^2}(\varepsilon_{xt} + \nu\varepsilon_{yt}) \tag{3a}$$

$$\sigma_{yt} = \frac{E}{1-\nu^2}(\varepsilon_{yt} + \nu\varepsilon_{xt}) \tag{3b}$$

$$\sigma_{xb} = \frac{E}{1-\nu^2}(\varepsilon_{xb} + \nu\varepsilon_{yb}) \tag{3c}$$

$$\sigma_{yb} = \frac{E}{1-\nu^2}(\varepsilon_{yb} + \nu\varepsilon_{xb}) \tag{3d}$$

where σ_{xt}、 σ_{yt} and σ_{xb}、 σ_{yb} are the normal stresses of the upper and lower body elements along the directions of the X-axis and the Y-axis of the global coordinate system, respectively. E is the elastic modulus. υ is poisson's ratio.

3.1.3. Shear strain of the micro-element

The shear strain will be generated under the influence of in-plane shear stresses based on the mechanical characteristics of the SBP. The deformation diagram is shown in Fig 5. According to the displacement of each point in Fig 5, the formulas for the shear strain at any point of the upper and lower elements can be respectively obtained:

$$\gamma_{xyt} = \frac{\partial u_t}{\partial y} + \frac{\partial v_t}{\partial x} = \frac{\partial u_{t0}}{\partial y} + \frac{\partial v_{t0}}{\partial x} - 2(z_1 + t/2)\frac{\partial^2 \omega}{\partial x \partial y} \tag{4a}$$

$$\gamma_{\mathrm{xyb}}=\frac{\partial u_{\mathrm{b}}}{\partial y}+\frac{\partial v_{\mathrm{b}}}{\partial x}=\frac{\partial u_{\mathrm{b0}}}{\partial y}+\frac{\partial v_{\mathrm{b0}}}{\partial x}-2(z_1+t/2)\frac{\partial^2\omega}{\partial x\partial y} \tag{4b}$$

According to Hooke's law [1], the shear stresses of the upper and lower elements are follows:

$$\tau_{\mathrm{xyt}}=G\gamma_{\mathrm{xyt}} \tag{5a}$$

$$\tau_{\mathrm{xyb}}=G\gamma_{\mathrm{xyb}} \tag{5b}$$

where the shear modulus of the material is $G=E/2(1+\nu)$.

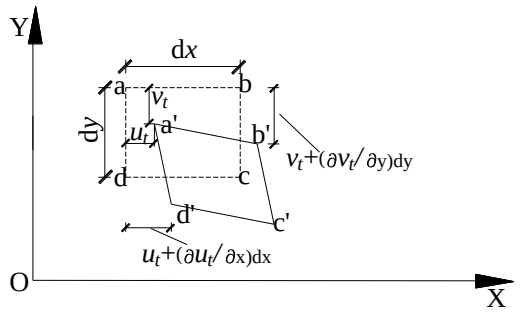

Fig. 5 Mechanism model of the shear strain

3.1.4. Shear slip of the connecting interface

In addition to self-deformation, the upper and lower elements also undergo shear slip deformation at their connection interfaces based on the geometric relationship shown in Fig. 3. The shear slip deformations can be decomposed into the shear slip deformation Δx and Δy along the X-axis and Y-axis directions, respectively.

$$\Delta_x=u_{\mathrm{b}}\big|_{z_1=0}-u_{\mathrm{t}}\big|_{z_1=0}=(u_{\mathrm{b0}}-u_{\mathrm{t0}})+t\frac{\partial\omega}{\partial x} \tag{6a}$$

$$\Delta_{\mathrm{y}}=v_{\mathrm{b}}\big|_{z_1=0}-v_{\mathrm{t}}\big|_{z_1=0}=(v_{\mathrm{b0}}-v_{\mathrm{t0}})+t\frac{\partial\omega}{\partial y} \tag{6b}$$

where Δ_x and Δ_y represent the shear slip deformation of the upper and lower elements along the X-axis and Y-axis of the global coordinate system, respectively.

3.1.5. Potential energy expression

According to the principle of energy conservation, the following equilibrium equation can be established:

$$\int_v\sigma_{ij}\varepsilon_{ij}\mathrm{d}V=U_1+U_2-W \tag{7}$$

where

$$U_1=\int_{V_1}[(\sigma_{\mathrm{xt}}\varepsilon_{\mathrm{xt}}+\sigma_{\mathrm{yt}}\varepsilon_{\mathrm{yt}}+\tau_{\mathrm{xyt}}\gamma_{\mathrm{xyt}})dV_1+\int_{V_2}[(\sigma_{\mathrm{xb}}\varepsilon_{\mathrm{xb}}+\sigma_{\mathrm{yb}}\varepsilon_{\mathrm{yb}}+\tau_{\mathrm{xyb}}\gamma_{\mathrm{xyb}})dV_2 \tag{8a}$$

$$U_2=\frac{K_{\mathrm{L}}}{2}\sum_{i=1}^{n}\int_{A_{si}}(\Delta_x^2+\Delta_y^2)dA_{si} \tag{8b}$$

$$W=\frac{\sigma}{2}\int_{V_1}[\frac{\partial u_{\mathrm{t}}}{\partial x}+(\frac{\partial\omega}{\partial x})^2]dV_1+\frac{\sigma}{2}\int_{V_2}[\frac{\partial u_{\mathrm{b}}}{\partial x}+(\frac{\partial\omega}{\partial x})^2]dV_2 \tag{8c}$$

where U_1 represents the sum of the bending potential energy of the two individual plates in the SBP; U_2 represents the total the potential energy of each shear element; W denotes the sum of external potential energy; V_1 and V_2 stand for the volumes of the upper plate and the lower plate; A_{si} represents the cross-sectional area of the i^{th} self-drilling screw; σ represents the compressive stress; and n represents the number of self-drilling screws.

The total potential energy expression of the SBP is derived according to equations (2)~(8).

$$\begin{aligned}\Pi&=U_1+U_2-W\\&=\frac{Et}{1-\nu^2}\int_0^a\int_0^b\frac{1}{2}\{[(\frac{\partial u_{\mathrm{t0}}}{\partial x}+\frac{\partial u_{\mathrm{b0}}}{x})+(\frac{\partial v_{\mathrm{t0}}}{\partial y}+\frac{\partial v_{\mathrm{b0}}}{\partial y})]^2+[(\frac{\partial u_{\mathrm{t0}}}{\partial x}-\frac{\partial u_{\mathrm{b0}}}{\partial x})+(\frac{\partial v_{\mathrm{t0}}}{\partial y}-\frac{\partial v_{\mathrm{b0}}}{\partial y})]^2\}dxdy+\\&\frac{Et^3}{12(1-\nu^2)}\int_0^a\int_0^b\{(\frac{\partial^2\omega}{\partial x^2}+\frac{\partial^2\omega}{\partial y^2})^2-2(1-\nu)[\frac{\partial^2\omega}{\partial x^2}\frac{\partial^2\omega}{\partial x^2}-(\frac{\partial^2\omega}{\partial x\partial y})^2]\}dxdy-\frac{Et^2}{1-\nu^2}\cdot\\&\int_0^a\int_0^b\frac{(1-\nu)}{2}\{[4\frac{\partial u_{\mathrm{t0}}}{\partial x}\frac{\partial v_{\mathrm{t0}}}{\partial y}-(\frac{\partial u_{\mathrm{t0}}}{\partial y}+\frac{\partial v_{\mathrm{t0}}}{\partial x})^2]+[4\frac{\partial u_{\mathrm{b0}}}{\partial x}\frac{\partial v_{\mathrm{b0}}}{\partial y}-(\frac{\partial u_{\mathrm{b0}}}{\partial y}+\frac{\partial v_{\mathrm{b0}}}{\partial x})^2]\}dxdy+\\&\frac{K_{\mathrm{L}}}{2}\sum_{i=1}^{n}\int_{A_{si}}\{[(u_{\mathrm{b0}}-u_{\mathrm{t0}})+t\frac{\partial\omega}{\partial x}]^2+[(v_{\mathrm{b0}}-v_{\mathrm{t0}})+t\frac{\partial\omega}{\partial y}]^2\}dA_{si}-\sigma t\int_0^a\int_0^b[\frac{1}{2}(\frac{\partial u_{\mathrm{t0}}}{\partial x}+\frac{\partial u_{\mathrm{b0}}}{\partial x})+(\frac{\partial\omega}{\partial x})^2]dxdy\end{aligned} \tag{9}$$

The shear slip influence parameters (u_{b0}, v_{b0}, u_{t0}, v_{t0}) between the two single plates and the constraint of self-drilling screws (the generalized stiffness K_{L}) are introduced in the total potential energy equation (9) in this paper. This can accurately reflect the mechanical characteristics of the SBP.

3.1.6. The critical stress of the coordinated buckling

The boundary conditions of the built-up plate with the four edges simply supported are as follows [1]:

$$\omega\big|_{x=0,x=a,y=0,y=b}=0 \tag{10a}$$

$$-D\frac{\partial^2\omega}{\partial y^2}\big|_{x=0,x=a,y=0,y=b}=0 \tag{10b}$$

where D represents the bending rigidity of the plate.

The deflection function [1] that satisfies equations (10a) - (10b) could be taken as:

$$\omega=A_1\sin(\frac{m\pi x}{a})\sin(\frac{\pi y}{b}) \tag{11a}$$

The displacement function satisfying the mid-plane boundary condition of

each single plate is:

$$u_{t0} = A_2 \frac{\partial \omega}{\partial x} \tag{11b}$$

$$u_{b0} = A_3 \frac{\partial \omega}{\partial x} \tag{11c}$$

$$v_{t0} = A_4 \frac{\partial \omega}{\partial y} \tag{11d}$$

$$v_{b0} = A_5 \frac{\partial \omega}{\partial y} \tag{11e}$$

where m is the number of the buckling half-wave; A_1、A_2、A_3、A_4 and A_5 are undetermined constants.

Substituting equations (10a)~(11e) into equation (9), and then perform the integration. A linear system of equations about $\partial\Pi/\partial A_1 = 0$, $\partial\Pi/\partial A_2 = 0$, $\partial\Pi/\partial A_3 = 0$, $\partial\Pi/\partial A_4 = 0$, $\partial\Pi/\partial A_5 = 0$ is established based on the principle of stationary potential energy. The condition for the system to have non-zero solutions is that the determinant of the coefficient matrix of this equation system is zero. The critical stress for the coordinated buckling of the SBP is then determined.

$$\sigma_{cr1} = k \frac{\pi^2 E}{12(1-\nu^2)} (\frac{\eta t}{b})^2 \tag{12}$$

where k is the stability coefficient of the SBP with four edges simply supported; η is the thickness reduction coefficient of the built-up plate reflecting the shear slip deformation and the influence of the self-drilling screw constraint. The formulas for these two parameters are:

$$k = (\frac{mb}{a} + \frac{a}{mb})^2 \tag{13a}$$

$$\eta = \sqrt{\frac{\pi^2 Et\sqrt{k} + 16aK_L(1-\nu^2)/me_1}{\pi^2 Et\sqrt{k} + 4aK_L(1-\nu^2)/me_1}} \tag{13b}$$

where a refers to the length of the plate. b refers to the width of the plate. m represents the half-wavelength of buckling. K_L represents the generalized stiffness parameter that reflects the constraint effect of self-drilling screws. e_1 refers to the screw spacing along the length of the plate.

3.2. Delamination buckling mode

The boundary conditions and the plate constraints inside the built-up plate have a significant influence on the mechanical characteristics of the SBP, as illustrated in Figs. 6(a)-6(b).

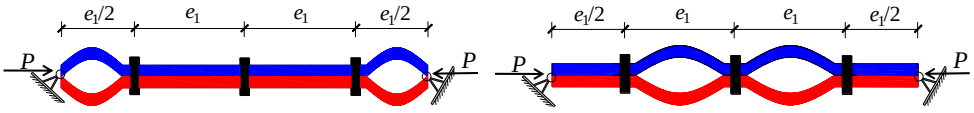

(a) End buckling (b) Inside buckling

Fig. 6 Buckling modes of the delamination buckling

3.2.1. calculation model

The calculation model is presented to analyze the mechanics characteristics of the delamination buckling of the SBP, as presented in Fig. 7.

The compression of each single plate is considered in both models. The angle and out-of-plane deflection are assumed to be close to "0", allowing for the further simplification of the complex deformation coordination and self-drilling screw constraint as the impact of the "boundary constraint condition" on the stability of the single plate.

Additionally, a critical half-wavelength is selected as the length of the SBP in the calculation model since the buckling behaviors are closely related to the buckling wavelength of members [17]. Meanwhile, this section also needs to meet the assumptions (1) and (2) outlined in Section 3.1.1 for further analysis.

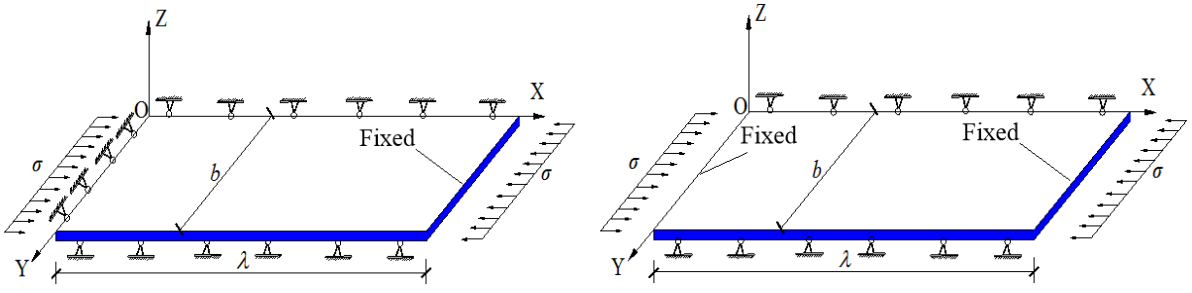

(a) End buckling (b) Inside buckling

Fig. 7 Calculation models of the delamination buckling

3.2.2. Potential energy expression

The total potential energy of the delamination buckling of the SBP consists of two parts: the bending strain energy and the external force potential energy:

$$\Pi = \frac{D}{2}\int_0^{\lambda}\int_0^{b}\{(\frac{\partial^2\omega}{\partial x^2}+\frac{\partial^2\omega}{\partial y^2})^2 + 2(1-\nu)[(\frac{\partial^2\omega}{\partial x\partial y})^2 - \frac{\partial^2\omega}{\partial x^2}\frac{\partial^2\omega}{\partial y^2}]\}dxdy - \frac{1}{2}\int_0^{\lambda}\int_0^{b}\sigma t(\frac{\partial\omega}{\partial x})^2 dxdy \tag{14}$$

where the flexural rigidity of the plate $D=Et^3/12(1-\nu^2)$; σ is the compressive stress; ω is the deflection along the Z-axis.

3.2.3. The critical stress of the delamination buckling

(1) End buckling

The boundary conditions [1] of the model in Fig. 7(a) are as follows:

$$\omega\big|_{x=0,x=\lambda,y=0,y=b} = 0 \tag{15a}$$

$$-D\frac{\partial^2\omega}{\partial y^2}\Big|_{x=0,y=0,y=b}=0 \tag{15b}$$

$$\frac{\partial\omega}{\partial x}\Big|_{x=\lambda}=0 \tag{15c}$$

The deflection function [27] that satisfies equations (17a)-(17c) can be expressed as:

$$\omega=A_1[\sin(\frac{2\pi x}{\lambda})+2\sin(\frac{\pi x}{\lambda})]\sin(\frac{\pi y}{b}) \tag{16}$$

By substituting the equations (15) and (16) into equation (14), the final buckling stress can be determined through simplification as follows:

$$\sigma_{f1}=k_{21}\frac{E\pi^2}{12(1-v^2)}(\frac{t}{b})^2 \tag{17a}$$

where the stability coefficient k_{21} is:

$$k_{21}=\frac{(20b^4+16b^2\lambda^2+5\lambda^4)}{8b^2\lambda^2} \tag{17b}$$

From this $\partial k_2/\partial\lambda=0$, it can get the critical half-wavelength as follows:

$$\lambda_{cr}=\sqrt{2}b\approx1.41b \tag{17c}$$

According to the influence of the screw spacing, the stability coefficient k_{21} is:

$$k_{21}=\begin{cases}4.5 & e_1>2.82b\\ \dfrac{(320b^4+64b^2{e_1}^2+5{e_1}^4)}{32b^2{e_1}^2} & e_1<2.82b\end{cases} \tag{17d}$$

(2) Inside buckling

The boundary conditions [1] of the model in Fig 7(b) are as follows:

$$\omega\Big|_{x=0,x=\lambda,y=0,y=b}=0 \tag{18a}$$

$$-D\frac{\partial^2\omega}{\partial y^2}\Big|_{y=0,y=b}=0 \tag{18b}$$

$$\frac{\partial\omega}{\partial x}\Big|_{x=0,x=\lambda}=0 \tag{18c}$$

The deflection function [26] that satisfies the equations (18a)-(18c) can be expressed as:

$$\omega=A_1\sin(\frac{\pi x}{\lambda})\sin(\frac{\pi x}{\lambda})\sin(\frac{\pi y}{b}) \tag{19}$$

Submitting the equations (18)-(19) into the equation (14), the inside buckling stress can be obtained through simplification as follows:

$$\sigma_{f2}=k_{22}\frac{E\pi^2}{12(1-v^2)}(\frac{t}{b})^2 \tag{20a}$$

where the stability coefficient k_{22} is:

$$k_{22}=\frac{(16b^4+8b^2\lambda^2+3\lambda^4)}{4b^2\lambda^2} \tag{20b}$$

From this $\partial k_{22}/\partial\lambda=0$, it can get the critical half-wavelength as follows:

$$\lambda_{cr}=\sqrt[4]{16/3}b\approx1.52b \tag{20c}$$

According to the influence of the screw spacing, stability coefficient k_{22} is:

$$k_{22}=\begin{cases}5.464 & e_1>1.52b\\ \dfrac{(16b^4+8b^2{e_1}^2+3{e_1}^4)}{4b^2{e_1}^2} & e_1<1.52b\end{cases} \tag{20d}$$

Therefore, from equations (17)-(20), the critical stress of the delamination buckling of the SBP is:

$$\sigma_{cr2}=k_2\frac{E\pi^2}{12(1-v^2)}(\frac{t}{b})^2 \tag{21a}$$

where the stability coefficient k_2 is the smaller of k_{21} and k_{22}, that is:

$$k_2=\min[k_{21},k_{22}] \tag{21b}$$

3.3. Comparison of coordinated buckling and delamination buckling

It can be observed from the instability mechanism that the members always progress towards the most unfavorable failure mode. Therefore, the CBS of the SBP should be smaller than the coordinated buckling and the delamination buckling, that is:

$$\sigma_{cr}=\min[\sigma_{cr1},\sigma_{cr2}] \tag{22}$$

where σ_{cr} represents the CBS of the SBP with the four edges simply supported; σ_{cr1} denotes the coordinated buckling stress, and σ_{cr2} indicates the delamination buckling stress.

It can be seen that the buckling deformation mode of the built-up plate must be determined before calculating the critical stress based on the above theoretical analysis. It is convenient for calculating the CBS.

Therefore, the thickness reduction coefficient (η) of the SBP in formula 13(b) should be combined with the stability coefficient (k) of the single plate. The stability coefficient of the SBP with four edges can be determined.

$$k_s=(\frac{mb}{a}+\frac{a}{mb})^2\frac{\pi^2Et(a/mb+mb/a)+16aK_L(1-v^2)/me_1}{\pi^2Et(a/mb+mb/a)+4aK_L(1-v^2)/me_1} \tag{23}$$

That is $\sigma_{cr1}=k_3\frac{E\pi^2}{12(1-v^2)}(\frac{t}{b})^2$. Therefore, only k_2 and k_3 need to be compared for the comparison of the CBSes of the coordinated buckling and the delamination buckling. Variables in k_2 are b and e_1. Variables in k_3 are b, e_1, and a. Hence, the relationship among the variables b, e_1, a, and k *is* discussed. The three-dimensional relationship of the b/a, e_1/a, and k in equations (21b) and (23) is illustrated in Fig. 8 to explore the determination of the buckling modes that occur in the SBP. It can be seen from Figs 8(a)-8(b) that the three-dimensional surface calculated by equation (21b) is always above the three-dimensional surface calculated by equation (23). In the case of the self-drilling screw arrangement shown in Fig. 3, the delamination buckling represents a higher order buckling mode of the coordinated buckling. Therefore, only the coordinated buckling is considered in the calculation of the CBS of the SBP. Thus, the CBS of the SBP with four edges simply supported is as follows:

$$\sigma = k\frac{E\pi^2}{12(1-v^2)}(\frac{\eta t}{b})^2 \quad (24)$$

where k is the stability coefficient of the single plate [1], and η is the thickness reduction coefficient of the SBP [5].

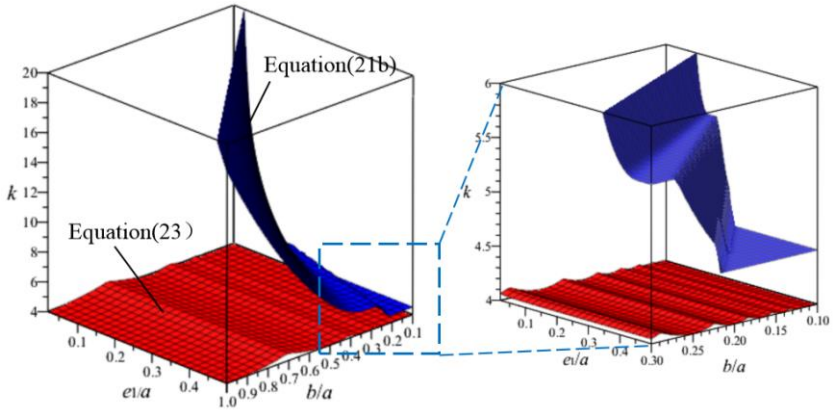

(a) Three-dimensional relationships for b/a, e_1/a and k at K= 100N/mm

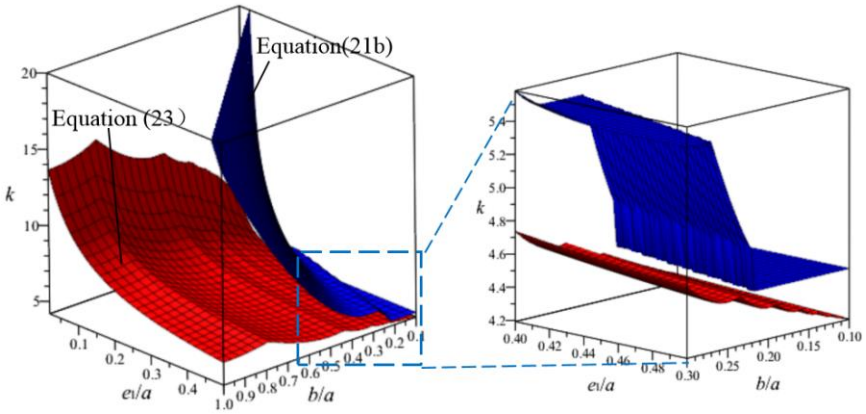

(b) Three-dimensional relationships for b/a, e_1/a and k at K= 90000N/mm

Fig. 8 Comparisons of the formula (21b) and the formula (23)

4. Reliability study

The SBP in this paper is extracted from the built-up web in the CFS back-to-back built-up column, as presented in Fig. 1. The constraint of the flanges on the webs is assumed to be a simply supported edge. The connection between the column ends and the end plates through spot welding is also considered as a simply supported boundary condition. Therefore, a screw built-up plate with simply supported on four sides is set up. This paper not only investigates the shear slip and screw constraint during the buckling of the SBP but also lays the foundation for subsequent works on CFS built-up columns.

The CFS built-up columns designed in this paper are divided into two series based on the different web heights: the 120 series and the 140 series. There are three different screw spacings for each different length of the CFS built-up columns. The screw spacing for the 120 series columns is 45mm, 90mm, and 150mm, respectively. The screw spacing for the 140 series columns is 50mm, 100mm, and 150mm, respectively. A total of 18 specimens were tested. The measured dimensions of the specimens are listed in Table 1. The representative positions of cross-sectional geometric dimensions are shown in Fig. 9, while naming rules for the members are illustrated in Fig. 10.

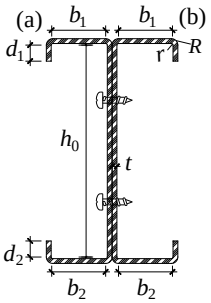

Fig. 9 Section diagram of specimens

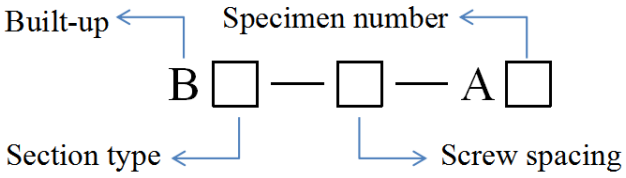

Fig. 10 Labeling rule of specimens

Table 1
The measured dimensions of the tested specimens

Specimens	Part	Measure length/mm	Geometric dimensions/mm						Outside diameter/mm	Inside diameter/mm
		L_s	h_0	b_1	b_2	d_1	d_2	t	R	r
B120-45-A1	a	367	114	55	54	23	15	1.22	4.0	2.8
	b	366	115.5	54.5	53.5	22.8	14.8	1.18	3.8	2.6
B120-45-A2	a	376	115	53	52	22	14	1.21	3.0	1.8
	b	376.5	115	55	54	23	15	1.18	4.0	2.8
B120-45-A3	a	369	115	54	53	22.5	14.5	1.21	3.5	2.3
	b	367	116	53	52	22	14	1.19	3.0	1.8
B120-90-A1	a	362	115	53	52	22	14	1.22	3.0	1.8
	b	366	115	54	53	22.5	14.5	1.22	3.5	2.3
B120-90-A2	a	380	116.5	53.5	52.5	22.3	14.3	1.17	3.3	2.1
	b	376	116	55	54	23	15	1.17	4.0	2.8
B120-90-A3	a	372.5	115.5	53.5	52.5	22.3	14.3	1.18	3.3	2.1
	b	370	115.5	53.5	52.5	22.3	14.3	1.17	3.3	2.1
B120-150-A1	a	367	116	52	51	21.5	13.5	1.22	2.5	1.3
	b	371.5	115	54	53	22.5	14.5	1.18	3.5	2.3
B120-150-A2	a	375	115	54	53	22.5	14.5	1.15	3.5	2.4
	b	374	115	56	55	23.5	15.5	1.17	4.5	3.3
B120-150-A3	a	364	114	54	53	22.5	14.5	1.22	3.5	2.3
	b	362	115	54	53	22.5	14.5	1.17	3.5	2.3
B140-50-A1	a	420.5	135	51.5	52.5	23.3	19.4	1.18	3.3	2.1
	b	420	135	51	52	23	19.1	1.19	3.0	1.8
B140-50-A2	a	420	136	51.5	52.5	23.3	19.4	1.18	3.3	2.1
	b	419.5	135.5	51.5	52.5	23.3	19.4	1.20	3.3	2.1
B140-50-A3	a	420	136	51	52	23	19.1	1.18	3.0	1.8
	b	420	134.5	52	53	23.5	19.6	1.20	3.5	2.3
B140-100-A1	a	419	135	52.5	53.5	23.8	19.9	1.15	3.8	2.6
	b	420	135	52	53	23.5	19.6	1.15	3.5	2.4
B140-100-A2	a	420	135.5	51.5	52.5	23.3	19.4	1.16	3.3	2.3
	b	415	135	52	53	23.5	19.6	1.16	3.5	2.3
B140-100-A3	a	420	136	51	52	23	19.1	1.22	3.0	1.8
	b	419.5	135	53	54	24	20.1	1.20	4.0	2.8
B140-150-A1	a	420	135	52.5	53.5	23.8	19.9	1.17	3.8	2.6
	b	420	135.5	51.5	52.5	23.3	19.4	1.16	3.3	2.1
B140-150-A2	a	418	138	50	51	22.5	18.6	1.17	2.5	1.3
	b	419	136	52	53	23.5	19.6	1.22	3.5	2.3
B140-150-A3	a	418.5	138	49	50	22	18.1	1.20	2.0	0.8
	b	421	136	50	51	22.5	18.6	1.17	2.5	1.3

The buckling characteristics of the test specimens are presented in Fig. 11. The buckling half-wave gradually appears on the specimen webs as the load increases. One of the built-up web plates undergoes convex deformation, while the other undergoes concave deformation. The coordination buckling phenomenon is becoming increasingly prominent under loading. The SBP undergoes coordinated buckling.

Additionally, this formula (24) is verified using data from the experiment, as listed in Table 2. The mean and standard deviation (SD) are 1.04 and 0.02, respectively. It can be seen that the calculated results are in good agreement with the experimental results. Therefore, it indicates that the study in this paper is accurate and reliable. In Table 2, σ_{crt} represents the experimental results. σ_{crc} represents the calculation results. The critical stress (σ_{crt}) is obtained based on the reverse point of strain, as detailed in the reference [4].

Table 2
Comparison of theoretical and experimental results

Specimens	σ_{crt}(N/mm^2)	σ_{crc}/(N/mm^2)	$\sigma_{crc}/\sigma_{crt}$
B120-45-A1	105.74	109.56	1.04
B120-45-A2	105.63	110.41	1.05
B120-45-A3	108.08	111.57	1.03

B120-90-A1	101.86	104.46	1.03
B120-90-A2	91.27	92.92	1.02
B120-90-A3	93.06	95.57	1.03
B120-150-A1	92.27	97.37	1.06
B120-150-A2	85.34	87.55	1.03
B120-150-A3	92.57	95.21	1.03
B140-50-A1	82.67	85.12	1.03
B140-50-A2	80.96	84.53	1.04
B140-50-A3	82.23	85.34	1.04
B140-100-A1	66.46	70.21	1.06
B140-100-A2	67.90	71.94	1.06
B140-100-A3	74.21	77.97	1.05
B140-150-A1	65.70	69.46	1.06
B140-150-A2	67.10	73.33	1.09
B140-150-A3	72.79	73.91	1.02
	Mean		1.04
	SD		0.02

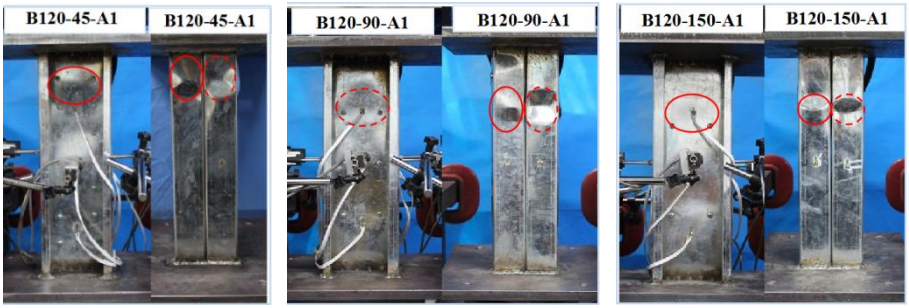

(a) 120 series built-up columns

(b) 140 series built-up columns

Fig. 11 Buckling characteristics of test specimens

5. The CBS of the SBP with other boundary conditions

Research has shown that the CBS of the SBP is closely related to the boundary conditions. These boundary conditions include the fixed at four sides, the two loading edges with simple support and two non-loading edges with fixed support, the two loading edges with fixed support, as well as two non-loading edges with simple support. The influence of the boundary constraint condition on the CBS of the SBP is discussed in this paper. The calculation model for the CBSes of the three boundary conditions of the SBP still refers to Fig. 1. Depending on the distinct boundary conditions, the displacement function [26] of the SBP can be approximated as follows:

(1) Fixed at four sides

$$\omega = \mathrm{A}\sin(\frac{m\pi x}{a})\sin(\frac{\pi x}{a})\sin(\frac{\pi y}{b})^2 \tag{25a}$$

(2) Two loading edges with simple support and two non-loading edges with fixed support

$$\omega = \mathrm{A}\sin(\frac{m\pi x}{a})\sin(\frac{\pi y}{b})^2 \tag{25b}$$

(3) Two loading edges with fixed support and two non-loading edges with simple support

$$\omega = \mathrm{A}\sin(\frac{m\pi x}{a})\sin(\frac{\pi x}{a})\sin(\frac{\pi y}{b}) \tag{25c}$$

The CBS of the coordinated buckling of the SBP can be obtained by referring to the above theoretical ideas.

$$\sigma = k\frac{E\pi^2}{12(1-\nu^2)}\left(\frac{\eta t}{b}\right)^2 \tag{26}$$

(1) Fixed at four sides

$$k=\frac{\pi^2(3b^4m^4+8a^2b^2m^2+18b^4m^2+16a^4+8a^2b^2+3b^4)}{3(m^2+1)a^2b^2} \tag{27a}$$

(2) Two loading edges with simple support and two non-loading edges with fixed support

$$k=\frac{16a^4+8a^2b^2m^2+16b^4m^4}{3m^2a^2b^4} \tag{27b}$$

(3) Two loading edges with fixed support and two non-loading edges with simple support

$$k=[\frac{b^2(m^4+6m^2+1)}{a^2(m^2+1)}+2+\frac{a^2}{b^2(m^2+1)}] \tag{27c}$$

It can be seen that the boundary conditions significantly affect the CBSes for the SBP. It can be proven that delamination buckling is still a higher order buckling mode of coordinated buckling under these boundary conditions. Therefore, only the coordinated buckling is considered when calculating the CBS of the SBP under the specified boundary conditions.

6. Conclusions and discussions

The influences of the coordinated buckling and delamination buckling on the CBS of the SBP are studied in this paper. The calculation models of the CBS are established. A calculation method for calculating the CBS of SBP is proposed. Therefore, the main conclusions can be drawn as follows:

(1) Delamination buckling always represents the higher-order mode of coordinated buckling when the SBP buckles. Based on the instability mechanism of the plate, it can be observed that the CBS of the SBP always consistently shifts towards the most unfavorable mode of development. Therefore, only the coordinated buckling should be considered when calculating the CBS of the screw built-up plate.

(2) The shear slip effect and the constraint effect of self-drilling screws are considered when deducing the CBS of the SBP. It indicates that the CBS is more accurate and closer to the actual situation of the SBP.

(3) The equation of the CBS for the SBP with four edges simply supported is derived and validated. However, the accuracy of the equations under different boundary conditions needs further verification.

(4) In this paper, it is proposed that the generalized stiffness K_L (shear stiffness) in the equation of the CBS of the SBP represents as the ability to prevent the sliding deformation of the plates along the connection interface. However, the theoretical analysis of shear stiffness needs to be further studied through experiments and theoretical study.

Authorship Statement derived and validated

Yanchun Li: Writing -original draft, Validation, Data curation; Tianhua Zhou: Supervision, Resources; Aihong Han: Writing - review & editing; Yan Lu: Writing -original draft; Jihao Chen: Software.

Acknowledgments

The authors are grateful to the financial support provided by the National Natural Science Foundation of China (No. 51878055), Key R&D and promotion projects in Henan Province (No. 242102321151) and (No. 242102321152), Key Scientific Research Projects of Universities (No. 23A560011) and (No. 22A560013).

References

[1] S.P. Timoshenko, J.M. Gere, Theory of Elastic Stability, 2nd ed. Mcgraw-Hill, New York, 1961.

[2] Lu Y, Zhou TH, Li WC, et al. On the plate assembly effects of compressed thin-walled C-section members at post-buckling stage. Journal of Huazhong University of Science and Technology (Natural Science Edition), 2017, 45(07):30-35 (In Chinese).

[3] Lu Y, Zhou TH, Li WC, et al. The critical local buckling load and ultimate strength of cold formed thin-walled C-sections under axial compression. Journal of Harbin Institute of Technology, 2017,49(06):72-76(In Chinese).

[4] Zhou TH, Li YC, Ren LJ, et al. Research on the elastic buckling of composite webs in cold-formed steel back-to-back built-up columns-Part I: Experimental and numerical investigation. Structures, 2021, 30:115-133.

[5] Li YC, Zhou TH, Ren LJ, et al. Elastic buckling of composite webs in back-to-back cold-formed steel built-up columns-Part II: Design formula. Structures, 2021, 33:3515-3525.

[6] Lu LF, Zhang YP, Fang WY, et al. Experimental investigation on shear-bearing capacity for self-drilling screw connections of cold-formed thin-walled steel. Journal of Central South University (Natural Science Edition), 2013, 44(07):2997-3005 (In Chinese).

[7] Shi Y, Wang SW, Liu YJ. Research on Shear Behavior of Single Tapping Screw Connection in Cold formed Thin-wall Steel Structures. Journal of Architecture and Civil Engineering, 2014, 31(02):57-64 (In Chinese).

[8] Roy K, Lau HH, Ting TCH. Experiments and finite element modelling of screw pattern of self-drilling screw connections for high strength cold-formed steel. Thin-Walled Structures, 2019, 145:106393.

[9] Li YC, Li RB, Zhou TH, et al. Novel design method of screwed connections of cold-formed steel built-up plates. Structures, 2023, 55:2433-2444.

[10] Huynh MT, Pham CH, Hancock GJ. Experimental behaviour and modelling of screwed connections of high strength sheet steels in shear. Thin-Walled Structures, 2020, 146:106357.

[11] Cai KY, Yuan HX. Testing, numerical and analytical modelling of self-drilling screw connections between thin steel sheets in shear. Thin-Walled Structures, 2023, 182:110292.

[12] Liu S, Feng RQ, Zhong YT. Experimental and numerical studies of screwed connections with hot-rolled steel plate and cold-formed steel sheet. Structures, 2023, 51:311-319.

[13] Liu WH, Deng L, Zhong WJ. Parametric study on the pull-out performance of screw connections in cold-formed thin-walled steel structures. Engineering Structures, 2023, 274:115007.

[14] Chen BS, Roy K. Uzzaman A. Axial strength of back-to-back cold-formed steel channels with edge-stiffened holes, un-stiffened holes and plain webs. J Constr Steel Res, 2020, 174:106313.

[15] Roy K, Ting TCH, Lau HH. Nonlinear behaviour of back-to-back gapped built-up cold-formed steel channel sections under compression. J Constr Steel Res, 2018, 147:257-76.

[16] Zhang JH, Young B. Experimental investigation of cold-formed steel built-up closed section columns with web stiffeners. J. Constr. Steel Res, 2018, 147:380-392.

[17] Roy K. Mohammadjani C, Lim JBP. Experimental and numerical investigation into the behaviour of face-to-face built-up cold-formed steel channel sections under compression. Thin-Walled Structures, 2019, 134:291-309.

[18] Dar MA, Subramanian N, Dar DA, et al. Flexural Strength of cold-formed steel built-up composite beams with rectangular compression flanges. Steel & Composite Structures, 2020, 34(2):171-188.

[19] Li YC, Zhou TH, Z L, et al. Distortional buckling behavior of cold-formed steel built-up closed section columns. Thin-walled Structures, 2021, 166:108069.

[20] Selvaraj S, Madhavan M. Experimental investigation and design considerations on cold-formed steel built-up I-section columns subjected to interactive buckling modes. Thin-Walled structures, 2022, 6:175.

[21] Ting TCH, Roy K, Lau HH. Effect of screw spacing on behavior of axially loaded back-to-back cold-formed steel built-up channel sections. Advances in Structural Engineering, 2018, 21(3):474-487.

[22] Wang LP, Young B. Behaviour and design of cold-formed steel built-up section beams with different screw arrangements. Thin-Walled Structures, 2018, 131:16-32.

[23] Chen BS, Roy K, Uzzaman A. Axial strength of back-to-back cold-formed steel channels with edge-stiffened holes, un-stiffened holes and plain webs. Journal of Constructional Steel Research, 2020, 174:106313.

[24] Fratamico DC, Torabian S, Zhao X. Experimental study on the composite action in sheathed and bare built-up cold-formed steel columns. Thin-Walled Structures, 2018, 127:290-305.

[25] Roy K, Lau HH, Ting TCH. Experiments and finite element modelling of screw pattern of self-drilling screw connections for high strength cold-formed steel. Thin-Walled Structures, 2019, 145:106393.

[26] Kechidi S, Fratamico DC, Schafer BW, et al. Simulation of screw connected built-up cold-formed steel back-to-back lipped channels under axial compression. Engineering Structures, 2020, 206:110109.

[27] Schafer, B. W. Cold-formed steel behavior and design: analytical and numerical modeling of elements and members with longitudinal stiffeners. New York: Cornell University. 1997.